A Variable-Length, Variable-Stiffness Soft Endoscope (VL-VS-SE) for Upper Gastrointestinal Tract

Heba Ali Mohsen[1], Alaa Al-Ibadi[2]*, Turki Y. Abdalla[3]

[1, 2, 3] Department of Computer Engineering, Engineering College, University of Basrah, Basrah, Iraq

Email: [1] engpg.heba.ali@uobasrah.edu.iq, [2] alaa.abdulhassan@uobasrah.edu.iq, [3] turki.abdalla@uobasrah.edu.iq

*Corresponding Author

Abstract— Endoscopy usually uses to investigate and diagnose numerous types of illnesses and infections. This procedure has been used successfully in the fields of thoracic surgery, urology, and in recent years gynecology. The process of Endoscopy occurs by inserting the endoscope inside the human body through the natural orifices of the body to diagnose health problems either in the upper gastrointestinal (GI) tract, which comprises the oral cavity, pharynx, esophagus, stomach, and small intestine, or the lower gastrointestinal (GI) tract, which includes of the large intestine and the anus. While the process is dealing with the soft organs, this article proposes a variable stiffness soft endoscope to ensure no impact on the human body is occurring. The endoscope is fully designed and manufactured by using a contraction pneumatic muscle actuator (PMA). The proposed device has the ability to change its length and stiffness. These features are controlled by experts. The system provides a live video by attaching a high-resolution camera at the front end.

Keywords— Endoscope, Mouth, Esophagus, PMA, Variable Length, Variable Stiffness, Human.

I. INTRODUCTION

The era of surgical robots officially began when the first Automated Endoscopic System for Optimal Positioning (AESOP), the voice-controlled camera holder prototype robot, after being employed in a surgical procedure in 1993, it was officially recognized by the US Administration of the Food and Drug as the pioneering surgical robot in 1994. The progress of Da Vinci's initial surgical prototype, introduced in 1997, had a significant impact on the advancement of minimally invasive surgery (MIS). This prototype has three arms—one for the camera and two for controlling tools—and functions as a master-slave manipulator, contributed greatly to the development of MIS.. After that, it evolved into one of the first truly intuitive surgical systems. This technology has shown to be ground-breaking and robust ever since it was created.[1]. The benefits of natural orifices transluminal surgery (NOTES), single-port procedures, and minimally invasive surgery (MIS) are well known and include a lower risk to patients, a shorter hospitalization, and a faster recovery time [2]. The majority of surgical tools- including those in the early stages of development - highly tend to be specific to a particular application and consequently only able to perform a limited range of surgical procedures. However, the majority of these instruments are rigid, do not have enough degrees of freedom (DOFs), and/or unable to change the mechanical characteristics to suit the task at hand [3]. Due to its soft nature, soft robotics technology is believed to be naturally safe for use in MIS. Contrarily, complicated control methods are needed for surgical robots made of stiff components to guarantee that the stresses placed on soft tissue are kept minimal and so minimize the chance of the patient being harmed. When using conventional rigid-component robots, computer faults, even though they are uncommon, can cause in uncontrollable robot arm motions, which could have disastrous effects on the patient[4]. So, the development of flexible surgical systems with numerous degrees of freedom or even continuous kinematics was the focus of several research projects, Among them are, De Flaco et, al.[5] designed an adjustable stiffness soft multi-module manipulator for MIS, this Stiff and Flop manipulator typically uses pneumatic power for actuation through the embedded fluidic chambers inside the modules, this design demonstrated its capacity to elongate and bend in all directions. Also, the design of the mesh worm soft robot is done by taking inspiration from the earthworm, this soft endoscope was created primarily for use during colonoscopies. Utilizing a new anchoring technique, the device is able to move ahead, orient the camera, and anchor using just one mechanism [6]. For MIS, [7] developed a highly maneuverable soft robot of two-module, and the effectiveness was assessed using a cadaver test, in which during a critical phase of a Total Mesorectal Excision (TME) treatment allowed the robot to navigate along anatomical characteristics and give a close-up picture of the site of surgery. This work presents the design, construction, and control of a variable length, variable stiffness soft endoscope (VL, VS, SE), this soft manipulator could help in the diagnosing of numerous types of illnesses and infections that occur in the upper gastrointestinal, especially for pharynx and esophagus. The rest of the article is partitioned into several sections. The second section briefly explains the human Pharynx and Esophagus and gives examples of possible diseases. The design of the proposed endoscope is illustrated in section three. Section four gives the operation and performance of the device. Finally, the conclusion and future work are explained in section five.

II.　HUMAN PHARYNX AND ESOPHAGUS

The main function of the esophagus is transporting food to the stomach from the pharynx. The food is usually be more liquidly during this mechanical process [8] [9]. Numerous diseases can affect this process by growing unwanted tissues or lack in mechanical behavior of the esophagus. Fig. 1 illustrates this section of the digestive system.

The esophagus has various main sectors. These include the cervical, thoracic and abdominal regions, as shown in Fig. 1. The neck part is the first region, and it is 5 – 6 cm in length. At its thinnest point, it has a diameter of 1.4 - 1.5 cm, with the residual sectors of the tissue having a diameter of nearly 2cm. Below the neck sector is the thoracic sector, which represents the greater part of the esophagus, and it is 16 – 18 cm in length. The abdominal region is the lower and tiniest region of the tissue that is 1 - 2.5 cm in length, varying according to the person size [8], [10], [11].

On the other hand, the second part of the digestive system after the mouth is the Pharynx. The deep cylinder in the interior of the neck that begins behind the nose and ends at the upper of the trachea and esophagus The pharynx is about 12 cm long and it is depends on the body size [8], [9], [12].

Achalasia, is an esophageal motility issue that cause decreased peristalsis in a body of the esophageal. Patients are suffering of vomiting, dysphagia, and pain around their chest [11], [13]. An efficient treatment for achalasia is a surgery [13], [14].
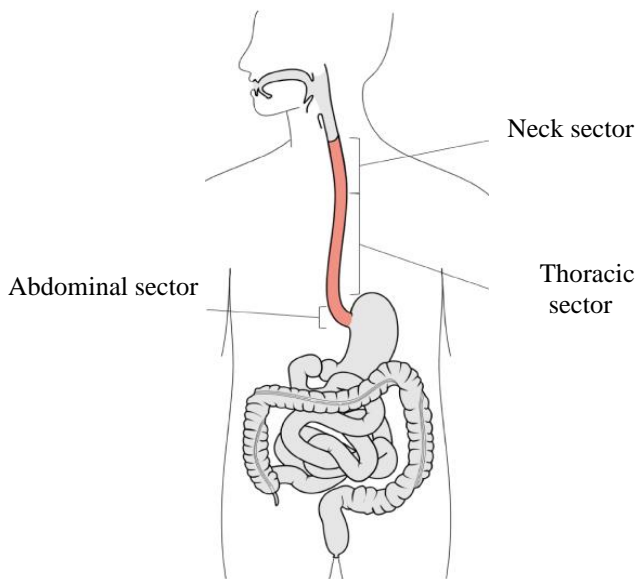

Fig. 1. The esophagus sectors of the human.

III.　ENDOSCOPE CONSTRUCTION

A single contraction pneumatic muscle actuator (PMA) is used to build the endoscope by using an inner rubber tube with outer diameter of 5.3 mm, and inner diameter of 2 mm. The length of the tube and the cover braided mesh is 350 mm. The minimum diameter of the braided mesh is 6 mm, and it is expanded up to 15 mm. Each of the internal bladder and the covered braided mesh are designed with similar lengths to create a contraction-type structure [15]–[17] [18][19]–[21] . Fig. 2, shows the construction of the contractor PMA.
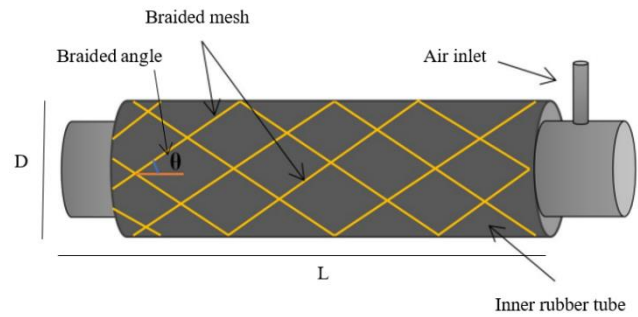

Fig. 2. The contractor PMA basic design.

Two end caps are used, one of them consists of a small inlet for air flow. 7mm Mini Camera (AN98, HD 720P, China) with a LED light is attached to the front-end for investigation.

The stiffness of the proposed endoscope is very low at no pressure, and it increases clearly by applying air pressure to the system. Since the utilized actuator is a contraction type, the stiffness of the endoscope rises when the air pressure is increasing. As well as, the diameter of the endoscope [22]–[25]. Fig. 3 illustrates the implemented device.

Fig. 3. A photograph of the VL-VS-SE.

To test the stiffness of the proposed device, various amounts of air pressure is applied in steps of 50 kPa. At each value, a load of 2 kg attached to the free end and the length difference is recorded by an ultrasonic sensor (see fig. 4). The stiffness is calculated by notice the length difference between the load and the no-load states and it is evaluated by (1):

$$s = f / \Delta L \qquad (1)$$

At equation (1), s refers to stiffness, f represents the applied force, and ΔL is the length deflection
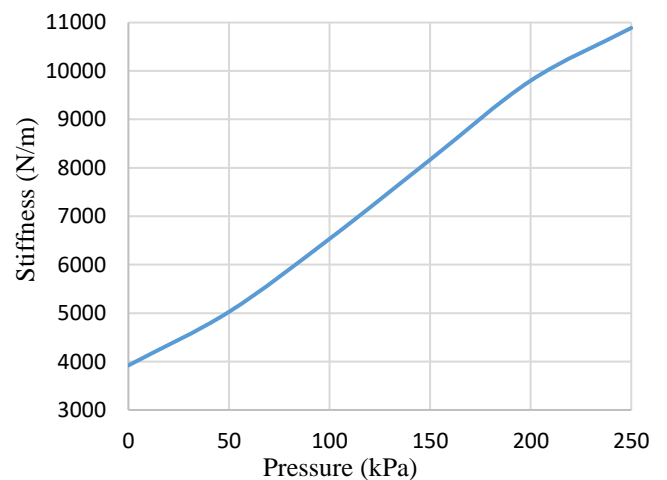

Fig. 4. The stiffness of the endoscope at 2 kg load.

Table I lists the length of the endoscope and the length difference at different air pressure values and 2 kg load.

TABLE I.
THE LENGTH AND ITS DEFLECTION OF THE ENDOSCOPE.

Pressure (kPa)	Length (m)	Length difference (m)
0	0.3	0.305
50	0.29	0.2939
100	0.27	0.273
150	0.25	0.2524
200	0.24	0.242
250	0.23	0.2318

IV.   OPERATION OF THE VL-VS-SE ING THE TEMPLATE

The proposed soft endoscope can be operated by specialists by adjusting the operation pressure to select the proper stiffness. At the beginning, the device shows no stiffness at all by the effect of the soft materials. Therefore, the user needs to increase the air pressure to maintain a linear shape.

This pose is required to insert the VL-VS-SE into the mouth. At this point, the pressure selected to be at its maximum limit, 200 kPa. This maximum operating pressure has been chosen experimentally as it shows a suitable posture for inserting the soft endoscope. Fig. 5 gives several postures of the endoscope at different air pressure values.

The attached camera can be operated by using an android phone or PC and adjust the light intensity manually.
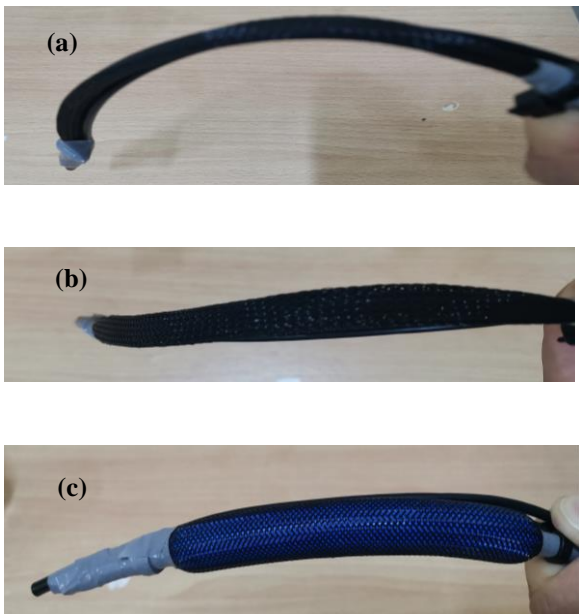

Fig. 5. The postures the endoscope. (a) The side view at no pressure. (b) The top view at no pressure. (c) The side view at 100 kPa. (d) The top view at 200 kPa.

Fig. 5 illustrates the relationship between stiffness and air pressure. Specifically, Figs. 5a and 5b depict the endoscope under low stiffness conditions. In Fig. 5c, the stiffness improves significantly at 100 kPa. The highest level of performance is observed in Fig. 5d.

V.   CONTROL SYSTEM

The designing process of a parallel Type-1 Mamdani model Fuzzy Logic Controller (FLC) system, in conjunction with PI controller will be presented in this section. The u(t) signal; which is the Pulse Width Modulation control signal; is the result of adding the signals from the two controllers, Fig. 6 shows The proposed controller's block diagram.
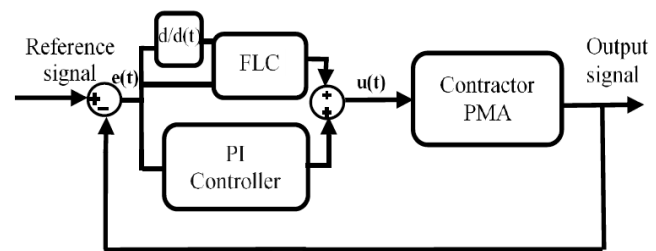

Fig. 6. The Adaptive Parallel Fuzzy Proportional Integral Controller (APFPIC) block diagram.

The initial stage of designing the fuzzy control system involves the fuzzification process, which entails defining the membership functions for the output and input variables. which will later be transformed into linguistic variables to fulfill the controller's objectives. In this process, the difference signal e(t) and its rate of change, de(t)/dt, serve as inputs to the fuzzy control system. The output variable from the FLC is represented by the air pressure amount. The fuzzy sets number assigned to each single variable usually based on the specific application of PMA and can range from 2 to 17. To ensure system stability, the two input variables' universe of discourse is established in the range of -6 to 6. Furthermore, the output variable domain spans from 0 to 250 kPa, in accordance with the SCPMA specification.

Additionally, each variable is divided into three fuzzy sets—Negative, Zero, and Positive—designated as N, Z, and P for the error variable, and Low, Medium, and High denoted as L, M, and H for the error-change variable. The output variable, representing the air pressure, is categorized into low-pressure, medium-pressure, and high-pressure, labeled as L, M, and H, respectively. In this case, the Gaussian membership function (MF) was selected for each of the input and the output variables. The Gaussian MF was chosen due to its simplicity and ability to prevent potential

discontinuities that may arise from mapping inputs/outputs of a Type-1 FLC.

In the subsequent stage, known as the inference engine, the intended output is produced by processing the fuzzy variables. The rule base is connected to this stage, where nine fuzzy rules are formulated in the format of "if x is A1 and y is B1, then z = C1." Here, both x and y represent the antecedents, while z denotes the consequent. The presented rules embody the knowledge and expertise of professionals in the specific field of applications. The control rules can be found in Table 2, which provides a visual representation of these rules.

TABLE II.
FUZZY RULES FOR THE APFPIC SYSTEM.

Error/Error change	Low	Medium	High
Negative	H	M	H
Zero	M	M	M
Positive	M	L	L

In the concluding phase, referred to as defuzzification, it is necessary to convert the fuzzy outputs into precise variables to achieve the desired control objectives. This conversion is of utmost importance. The center of gravity (CoG) approach is utilized in this stage to reverse the process of the fuzzy logic. It determines the centroid by evaluating the area under the MF, as depicted in (2). The result from this step describes the air pressure, which is representing by the Pulse Width Modulation signal (PWM).

$$CoG(X) = \frac{\sum_{i=1}^{\mu} \mu_i(x) X_i}{\sum_{i=1}^{\mu} \mu_i} \qquad (2)$$

Where $\mu_i(x)$ represents the combined output membership function.

To enhance tracking performance in steady state, the proposed controller incorporates an integrator. However, the conventional constant gain PI controller struggled to handle uncertainties and parametric fluctuations, especially in fluidic systems. Consequently, the FLC was introduced to address the need for performance improvement by addressing the nonlinearity and complexity of SCPMA dynamic behaviors.

The PWM duty cycle generated by both the PI and FLC controllers serves as the output signal for the Adaptive Proportional-Integral-Fuzzy Inference Control (APFPIC) controller. This signal is utilized to control the quantity of pressurized air, ranging between 0 kPa to 250 kPa, which is then employed to inflate the 30 cm contractor actuator. The control system was theoretically simulated with square wave input signal and the results are illustrated in Fig. 7.

This figure depicts the behavior of the control signal representing the pressurized air as a function of time for a square wave signal. The APFPIC controller demonstrated adaptive and precise responses, effectively reducing steady-state error and improving transient performance. In Fig. 7, the

system output is illustrated in response to a square wave reference input, fluctuating between 100 kPa and 200 kPa.
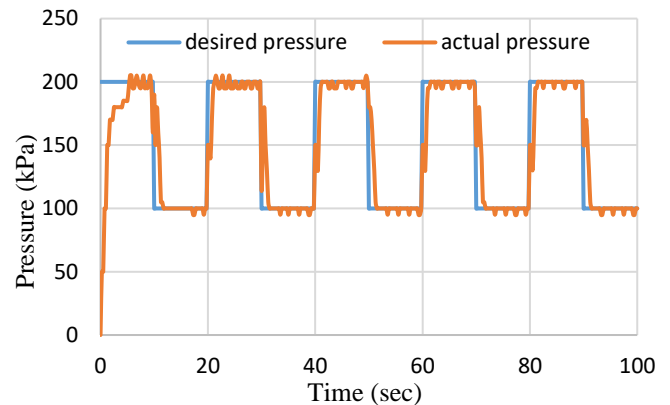

Fig. 7. The reference and the system response for a square wave signal.

Fig. 7 demonstrates the controller system's performance in achieving the desired functionality of the contraction actuator. Despite the presence of a small steady-state error, the hysteresis performance ensures that it does not significantly impact the behavior of the endoscope [21] [26]–[30] [31].

VI.   CONCLUSIONS

In this research article, a soft endoscopy device designed for investigating the Pharynx and Esophagus is presented. The device consists of a soft contraction actuator and a small camera with adjustable lighting. The pneumatic muscle actuator used in the device offers enhanced safety during human interaction due to its soft and low stiffness properties, in contrast to rigid actuators. This type of actuator exhibits varying stiffness behavior based on the air pressure applied. Experts can utilize the endoscope device by adjusting the air pressure to increase stiffness, thereby maintaining a linear shape, and subsequently reducing the air pressure as needed.

To regulate the air pressure and adjust the stiffness of the device, a hybrid control system comprising both PI and Fuzzy controllers is employed simultaneously. The Adaptive Parallel Fuzzy Proportional Integral Controller (APFPIC) is tested under two pressure states, specifically at 100 kPa and 200 kPa. In future developments, experts can conduct testing on humans at clinics using the presented device, the VL-VS-SE. Its length can be extended to enable investigation of the entire digestive system.

REFERENCES

[1]   J. H. Palep, "Robotic assisted minimally invasive surgery," *J. Minim. Access Surg.*, vol. 5, no. 1, p. 1, 2009.

[2]   C. J. Hawkey, J. Bosch, J. E. Richter, G. Garcia-Tsao, and F. K. L. Chan, *Textbook of clinical gastroenterology and hepatology*. John Wiley & Sons, 2012.

[3]   A. Loeve, P. Breedveld, and J. Dankelman, "Scopes too flexible... and too stiff," *IEEE Pulse*, vol. 1, no. 3, pp. 26–41, 2010.

[4]   K. W. Kwok, H. Wurdemann, A. Arezzo, A. Menciassi, and K. Althoefer, "Soft Robot-Assisted Minimally Invasive Surgery and Interventions: Advances and Outlook," *IEEE Trans. Robot.*, 2022.

[5]   I. De Falco, M. Cianchetti, and A. Menciassi, "STIFF-FLOP surgical manipulator: design and preliminary motion evaluation," in *Proc. 4th Workshop Computer/Robot Assisted Surgery (CRAS)*, 2014, pp. 131–134.

[6]   J. E. Bernth, A. Arezzo, and H. Liu, "A novel robotic meshworm with segment-bending anchoring for colonoscopy," *IEEE Robot. Autom. Lett.*, vol. 2, no. 3, pp. 1718–1724, 2017.

[7]   H. Abidi *et al.*, "Highly dexterous 2-module soft robot for intra-organ navigation in minimally invasive surgery," *Int. J. Med. Robot. Comput. Assist. Surg.*, vol. 14, no. 1, p. e1875, 2018.

[8]   C. Durcan *et al.*, "Experimental investigations of the human oesophagus: anisotropic properties of the embalmed mucosa–submucosa layer under large deformation," *Biomech. Model. Mechanobiol.*, vol. 21, no. 6, pp. 1685–1702, Dec. 2022, doi: 10.1007/s10237-022-01613-1.

[9]   C. Cock and T. Omari, "Systematic Review of Pharyngeal and Esophageal Manometry in Healthy or Dysphagic Older Persons (>60 years)," *Geriatrics*, vol. 3, no. 4, p. 67, Oct. 2018, doi: 10.3390/geriatrics3040067.

[10]   C. M. Knauer, J. A. Castell, C. B. Dalton, L. Nowak, and D. O. Castell, "Pharyngeal/upper esophageal sphincter pressure dynamics in humans," *Dig. Dis. Sci.*, vol. 35, no. 6, pp. 774–780, 1990, doi: 10.1007/bf01540183.

[11]   M. S. Levine and S. E. Rubesin, "History and Evolution of the Barium Swallow for Evaluation of the Pharynx and Esophagus," *Dysphagia*, vol. 32, no. 1, pp. 55–72, Feb. 2017, doi: 10.1007/s00455-016-9774-y.

[12]   Y. Khalifa, C. Donohue, J. L. Coyle, and E. Sejdic, "Upper Esophageal Sphincter Opening Segmentation with Convolutional Recurrent Neural Networks in High Resolution Cervical Auscultation," *IEEE J. Biomed. Heal. Informatics*, vol. 25, no. 2, pp. 493–503, 2021, doi: 10.1109/JBHI.2020.3000057.

[13]   H. Shiwaku and H. Inoue, "Recent advancement of submucosal endoscopy: Peroral endoscopic myotomy and offshoot," *Dig. Endosc.*, vol. 34, no. S2, pp. 36–39, May 2022, doi: 10.1111/den.14155.

[14]   S. Kiuchi, J. Sasaki, T. Arai, and T. Suzuki, "Functional Disorders of the Pharynx and Esophagus," *Acta Otolaryngol.*, vol. 68, no. sup256, pp. 1–30, Jan. 1969, doi: 10.3109/00016486909129232.

[15]   A. Al-Ibadi, S. Nefti-Meziani, and S. Davis, "The Design, Kinematics and Torque Analysis of the Self-Bending Soft Contraction Actuator," *Actuators*, vol. 9, no. 2, p. 33, Apr. 2020, doi: 10.3390/act9020033.

[16]   T. Park and Y. Cha, "Soft mobile robot inspired by animal-like running motion," *Sci. Rep.*, vol. 9, no. 1, p. 14700, Dec. 2019, doi: 10.1038/s41598-019-51308-4.

[17]   A. Al-Ibadi, S. Nefti-Meziani, and S. Davis, "Controlling of Pneumatic Muscle Actuator Systems by Parallel Structure of Neural Network and Proportional Controllers (PNNP)," *Front. Robot. AI*, vol. 7, Oct. 2020, doi: 10.3389/frobt.2020.00115.

[18]   D. Rus and M. T. Tolley, "Design, fabrication and control of soft robots," *Nature*, vol. 521, no. 7553, pp. 467–475, May 2015, doi: 10.1038/nature14543.

[19]   T. George Thuruthel, Y. Ansari, E. Falotico, and C. Laschi, "Control Strategies for Soft Robotic Manipulators: A Survey," *Soft Robot.*, vol. 5, no. 2, pp. 149–163, Apr. 2018, doi: 10.1089/soro.2017.0007.

[20]   M. Manti, T. Hassan, G. Passetti, N. D'Elia, C. Laschi, and M. Cianchetti, "A Bioinspired Soft Robotic Gripper for Adaptable and Effective Grasping," *Soft Robot.*, vol. 2, no. 3, pp. 107–116, Sep. 2015, doi: 10.1089/soro.2015.0009.

[21]   M. E. Giannaccini, C. Xiang, A. Atyabi, T. Theodoridis, S. Nefti-Meziani, and S. Davis, "Novel Design of a Soft Lightweight Pneumatic Continuum Robot Arm with Decoupled Variable Stiffness and Positioning," *Soft Robot.*, 2018, doi: 10.1089/soro.2016.0066.

[22]   H. A. Mohsen, A. Al-Ibadi, and T. Y. Abdalla, "Different Types of Control Systems for the Contraction Pneumatic Muscle Actuator," in *2022 8th International Conference on Control, Decision and Information Technologies (CoDIT)*, May 2022, pp. 956–961, doi: 10.1109/CoDIT55151.2022.9804047.

[23]   B. Kalita, A. Leonessa, and S. K. Dwivedy, "A Review on the Development of Pneumatic Artificial Muscle Actuators: Force Model and Application," *Actuators*, vol. 11, no. 10, p. 288, Oct. 2022, doi: 10.3390/act11100288.

[24]   H. Al-Mosawi, A. Al-Ibadi, and T. Abdalla, "A Comprehensive Comparison of Different Control Strategies to Adjust the Length of the Soft Contractor Pneumatic Muscle Actuator," *Iraqi J. Electr. Electron. Eng.*, vol. 18, no. 2, pp. 101–109, Dec. 2022, doi: 10.37917/ijeee.18.2.13.

[25]   A. Al-Ibadi, S. Nefti-Meziani, and S. Davis, "Efficient Structure-Based Models for the McKibben Contraction Pneumatic Muscle Actuator: The Full Description of the Behaviour of the Contraction PMA," *Actuators*, vol. 6, no. 4, p. 32, Oct. 2017, doi:

10.3390/act6040032.

[26]   K. H. Ang, G. Chong, and Y. Li, "PID control system analysis, design, and technology," *IEEE Trans. Control Syst. Technol.*, vol. 13, no. 4, pp. 559–576, 2005.

[27]   J. Fan, J. Zhong, J. Zhao, and Y. Zhu, "BP neural network tuned PID controller for position tracking of a pneumatic artificial muscle," *Technol. Heal. Care*, vol. 23, pp. S231–S238, 2015, doi: 10.3233/THC-150958.

[28]   T. K. Shen, I. F. Lee, P. H. Lin, C. I. Lin, P. C. Lin, and W. P. Shih, "Implementation of a PID controller for a robotic leg actuated by pneumatic artificial muscles," 2015, doi: 10.6567/IFToMM.14TH.WC.OS13.086.

[29]   G. Andrikopoulos, G. Nikolakopoulos, and S. Manesis, "Advanced nonlinear PID-based antagonistic control for pneumatic muscle actuators,"

IEEE Trans. Ind. Electron., vol. 61, no. 12, pp. 6926–6937, 2014, doi: 10.1109/TIE.2014.2316255.

[30]   T. D. C. Thanh and K. K. Ahn, "Nonlinear PID control to improve the control performance of 2 axes pneumatic artificial muscle manipulator using neural network," *Mechatronics*, vol. 16, no. 9, pp. 577–587, Nov. 2006, doi: 10.1016/j.mechatronics.2006.03.011.

[31]   A. Al-Ibadi, S. Nefti-Meziani, and S. Davis, "A circular pneumatic muscle actuator (CPMA) inspired by human skeletal muscles," in *2018 IEEE International Conference on Soft Robotics (RoboSoft)*, Apr. 2018, pp. 7–12, doi: 10.1109/ROBOSOFT.2018.8404889.